Available online at www.sciencedirect.com
ScienceDirect
Journal of Sound and Vibration 312 (2008) 442–460
JOURNAL OF SOUND AND VIBRATION
www.elsevier.com/locate/jsvi

Linear and nonlinear 2D finite element analysis of sloshing modes and pressures in rectangular tanks subject to horizontal harmonic motions

Juan C. Virella[a], Carlos A. Prato[b], Luis A. Godoy[b,*]

[a]Department of Civil Engineering and Surveying, University of Puerto Rico, Mayagüez, PR 00681-9041, USA
[b]Structures Department, FCEF y N, National University of Cordoba, Casilla de Correo 916, Cordoba 5000, Argentina

Received 22 September 2004; received in revised form 11 April 2007; accepted 10 July 2007
Available online 20 February 2008

Abstract

The influence of nonlinear wave theory on the sloshing natural periods and their modal pressure distributions are investigated for rectangular tanks under the assumption of two-dimensional behavior. Natural periods and mode shapes are computed and compared for both linear wave theory (LWT) and nonlinear wave theory (NLWT) models, using the finite element package ABAQUS. Linear wave theory is implemented in an acoustic model, whereas a plane strain problem with large displacements is used in NLWT. Pressure distributions acting on the tank walls are obtained for the first three sloshing modes using both linear and nonlinear wave theory. It is found that the nonlinearity does not have significant effects on the natural sloshing periods. For the sloshing pressures on the tank walls, different distributions were found using linear and nonlinear wave theory models. However, in all cases studied, the linear wave theory conservatively estimated the magnitude of the pressure distribution, whereas larger pressures resultant heights were obtained when using the nonlinear theory. It is concluded that the nonlinearity of the surface wave does not have major effects in the pressure distribution on the walls for rectangular tanks.

1. Introduction

Rectangular tanks are commonly used to store water and various fluids in the oil industry. Damage in tanks may cause a loss of liquid content, which could result in economic damage, as well as in long-term contamination of soil. In some cases, water storage tanks are part of a fire-fighting system, so that the interruption of the water system may result in additional damage due to fire. Abundant research has been made on the seismic response of cylindrical storage tanks, but few contributions have been published for rectangular tanks, as stated by Koh et al. [1].

Housner [2] solved analytically the Laplace equation for the fundamental mode of rectangular and cylindrical rigid tanks resting on rigid foundations, under horizontal ground excitation and considering linear wave theory (LWT). Housner [2] established that the hydrodynamics of liquids in rigid tanks can be divided in

*Corresponding author. Tel.: +54 787 265 3815; fax: +54 787 833 8260.
E-mail address: lgodoy@uprm.edu (L.A. Godoy).

0022-460X/$ - see front matter © 2007 Elsevier Ltd. All rights reserved.
doi:10.1016/j.jsv.2007.07.088

an impulsive and a sloshing component. The liquid in the upper part has sloshing motion with a long period of vibration, whereas the rest of the fluid moves with the tank in an impulsive mode. A generalized two-degree of freedom system was proposed to represent the impulsive and sloshing modes of vibration. Haroun [3] assumed a rigid structure and studied the hydrodynamic response of rectangular tanks considering linear wave theory.

Most of the studies that followed Housner considered the seismic response of cylindrical tanks, and were later expanded to take into account the effect of the flexibility of the tank wall into the hydrodynamic pressure that results from the impulsive mode. Veletsos [4,5], Veletsos and Yang [6], and Haroun and Housner [7] developed flexible anchored tank linear models, and found that the pressure distributions for the impulsive mode of rigid and flexible tanks were similar, but also discovered that the magnitude of the pressure was highly dependent on the wall flexibility. Kim et al. [8] included the flexibility of the structure to study the impulsive response of rectangular tanks, whereas the sloshing response was neglected.

For the sloshing component of cylindrical steel tanks, Veletsos [5] stated that the effect of the flexibility of the tank does not change the pressure distribution on the walls, due to the large differences between the fundamental periods of the earthquake excitation and the periods required to form sloshing waves. Therefore, the assumption of rigid tank is a good approximation to evaluate the hydrodynamic pressures due to the sloshing component of the liquid in cylindrical tanks. Koh et al. [1] analyzed the dynamic response of three-dimensional (3D) liquid storage rectangular concrete tanks, considering linear wave theory, and found that the sloshing response can be amplified due to the flexibility of the tank. For tanks with thicker walls, a response similar to the rigid tank was obtained.

Choun and Yun [9] studied the sloshing response of rectangular tanks with a submerged structure considering linear wave theory, and subjected to horizontal ground excitations. Sloshing peak wave amplitudes from time history analyses and response spectra were obtained for various models subjected to the earthquake records of El Centro NS (1940), El Centro EW (1940), Loma Prieta (1989), and Mexico City (1985). With the exception of the Mexico City record (1985), the contribution of the first sloshing mode to the surface wave amplitude was very high, in the range between 80% and 99%. For the Mexico City earthquake, the contributions of the first mode to the surface wave amplitude were smaller (from 43% to 68%), and higher sloshing modes were necessary to accurately predict the sloshing wave amplitude, because the predominant frequency of the earthquake was closer to the second sloshing mode.

Veletsos and Shivakumar [10] obtained the sloshing natural periods and corresponding mode shapes for cylindrical tanks, with linear elasticity assumption. Newmark and Rosenblueth [11] stated that for high surface waves a nonlinear relation between the hydrodynamic pressure and the surface wave displacement needs to be considered. The maximum surface wave amplitudes with linear and nonlinear wave theory for harmonic horizontal motions are not addressed in our paper, since it turned out from this investigation that the natural frequencies and resulting modal pressures are rather insensitive to wave amplitudes, and therefore interest was focused on showing how the pressure distribution changes as nonlinearity is considered. The surface wave amplitude could be larger as nonlinearity is included in the sloshing analysis, but the question of whether the pressure distribution changes significantly with respect to linear wave theory remains to be answered.

This paper reports results on the evaluation of natural periods and pressures due to sloshing using conventional finite element tools. The specific interest is in assessing the importance of nonlinear wave theory as opposed to a model with a linearized relation between wave height and wall pressures. The analysis is carried out for rectangular tanks with different liquid height to tank width ratios. The effect of the tank geometry and the level of liquid on the natural sloshing periods and corresponding pressures are investigated.

2. Tank–liquid systems

Rectangular tank–liquid systems may be modeled as plane strain problems, in which one of the dimensions is much larger than the other, as illustrated in Fig. 1. The main assumptions of the present model are: (a) the tank is assumed to be rigid, so that there is no elastic interaction between the tank and the liquid; and (b) the tank is assumed to rest on rock, so that soil–structure interaction is not included in the analysis. To illustrate the behavior of such systems, rectangular tanks with different liquid height to width ratios were considered,

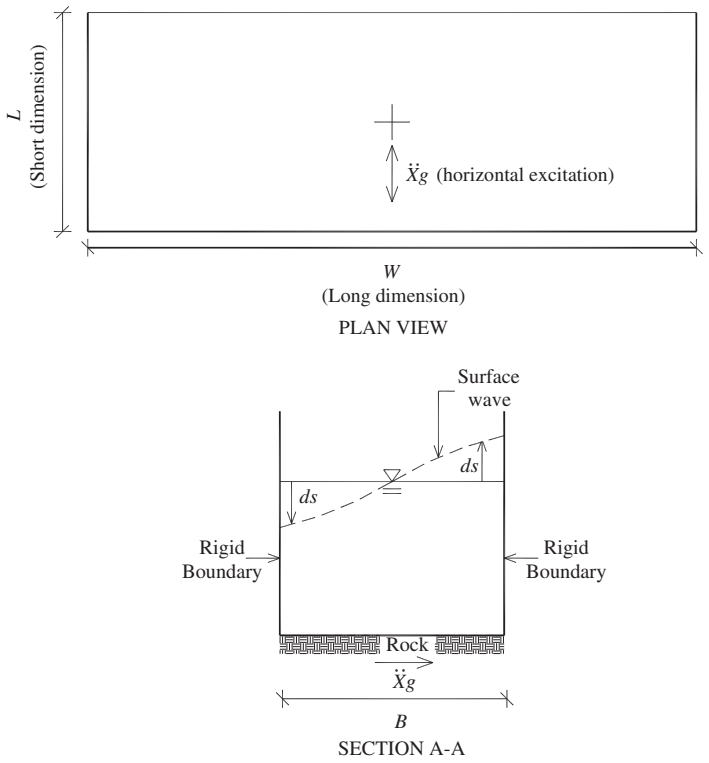

Fig. 1. Notation for the 2D plane rectangular model of the tank–liquid system.

Table 1
Parameters of the tank–liquid systems considered

Model	H_L (m)	H_L/R
1	6.10	0.40
2	8.46	0.56
3	9.62	0.63
4	10.73	0.70
5	13.31	0.87
6	14.51	0.95
7	16.70	1.10
8	19.33	1.27
9	25.20	1.65

Notes: H_L = liquid level height, $R = B/2$, B = tank width.

where the notation is shown in Fig. 1, and the data used is in Table 1. It is assumed that the tanks are filled with water, with density (ρ) = 983 kg/m^3 and bulk modulus (K) = 2.07×10^9 Pa.

2.1. Model assuming linear wave theory

An acoustic model is used in this work for the linear wave theory analysis. A continuum is said to be acoustic if it can be described using just compression and expansion without any shear effect. The dilatational motion allows a wave to be described as a single pressure degree of freedom at any point in space. Some viscosity effects can also be considered, although an inviscid liquid is assumed in our case. Reactive boundary conditions are specified at the liquid surface, where the sloshing action takes place for small pressure changes.

For an acoustic medium, Ref. [12] presents the continuity or strain compatibility equation for 1D motion. For 2D motions assuming inviscid and isotropic fluid, the continuity or volumetric strain compatibility equation of the fluid can be written as

$$\frac{\partial^2 P}{\partial x^2}+\frac{\partial^2 P}{\partial y^2}-\frac{\rho}{K}\frac{\partial^2 P}{\partial t^2}=0, \tag{1}$$

where P is the pressure, positive in compression; x, y, the Cartesian coordinates; and t the time. Eq. (1) has the same form as the Laplace equation in the pressure domain. The incompressibility assumption has not been explicitly included, however for common dimensions of liquid containments, near incompressible behavior occurs.

The constitutive relationship for the material takes the linear form

$$P=-K\varepsilon_v, \tag{2}$$

where ε_v is the volumetric strain. The volumetric strain compatibility equation (Eq. (1)), is solved using 2D finite elements with a mesh discretization of 560 elements and 609 degrees of freedom (Fig. 2). The elements for the liquid are identified in ABAQUS [13] as AC2D4, which is a solid, four node, and plane strain acoustic element with bilinear interpolation, having only one pressure unknown per node. With reference to Fig. 2, the boundary conditions used to solve the volumetric strain compatibility equation in Ref. [12] are

1. At the bottom boundary, the normal acceleration ($\ddot{u}_n$) in the normal direction n, is specified:
$$\frac{\partial P}{\partial n}=-\rho\ddot{u}_n. \tag{3}$$
Because the input acceleration (nodal load in an acoustic environment) is horizontal, the normal acceleration ($\ddot{u}_n$) for this boundary is zero.
2. *Rigid wall boundary*: Because the input acceleration is horizontal, the normal acceleration for this boundary in Eq. (3) is taken as the horizontal acceleration at the base.
3. The boundary at the top is a reactive boundary, in which the pressure of the acoustic medium varies because of the normal motion of the boundary. It is assumed that the acoustic particle velocity in the outward normal direction of the fluid surface ($\dot{u}_{\text{out}}$) is related to the pressure and the time rate of change of the pressure as [12]
$$\dot{u}_{\text{out}}=\frac{1}{K_1}\frac{\partial P}{\partial t}+\frac{1}{c_1}P, \tag{4}$$
where $\dot{u}_{\text{out}}$ is the outward normal velocity at the boundary; K_1 the proportionality factor between the normal velocity and the time rate of change of the pressure, which depends on the acoustic reactive surface; c_1 the proportionality factor between the normal velocity and the pressure, which depends on the acoustic reactive surface. In the case of a sloshing reactive surface, the proportionality factors are $c_1=0$, $K_1=\rho g$ (g = acceleration of gravity = 9.81 m/s^2). For the case of sloshing, the boundary condition in

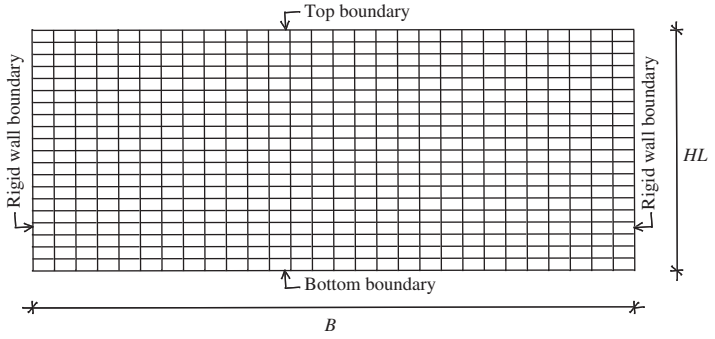

Fig. 2. Typical finite elements mesh for the tank–liquid system of the 2D sloshing model; H_L = liquid height; B = tank width.

Eq. (4) shows the relation of the liquid surface pressure with the sloshing wave amplitude formed. To explicitly show this relationship, Eq. (4) can be written as

$$d_s = \frac{P}{\rho g}, \tag{5}$$

where d_s is the surface wave height.

The sloshing waves in the models form due to gravity, as a consequence of Eq. (5); so in the absence of gravity, no sloshing waves would form at the liquid surface due to the excitation.

A steady-state harmonic analysis (direct integration) considering linear wave theory was used to find the natural sloshing periods and mode shapes of the tank–liquid systems. The dynamic response is obtained as a function of the load frequency, and the natural frequencies are defined as those associated with the peaks of response, and at those frequencies the pressure distributions are obtained (i.e., in each step in the analysis the harmonic loads were tuned to a specific frequency and results obtained) for each mode. The solution of the problem in term of P yields a deformed shape associated with the modal pressure distribution in the tank. A plot of the pressure variation at the liquid surface denotes the oscillating liquid surface that characterizes the mode. The pressure distribution on the rigid wall is the sloshing pressure on the tank walls due to the sloshing waves. Normal accelerations (a_n) equal to unity were specified at the rigid wall boundaries (Fig. 2), and different steps were solved, in which the acceleration frequency changed automatically, and response curves (showing the variation between the response pressure and the excitation frequency) were plotted. The sloshing natural periods were obtained from the peaks of response curves of natural period versus maximum surface wave pressure, obtained for each of the tank–liquid systems considered.

2.2. Model assuming nonlinear wave theory

The need to include nonlinear wave theory in the hydrodynamics of the tank–liquid system arises whenever high amplitude sloshing waves form on the liquid surface, leading to a nonlinear influence of surface pressure and sloshing wave on the pressure distribution on the rigid walls.

Nonlinear wave theory is modeled in this paper as a 2D plane strain problem with geometric nonlinear behavior, and the results are given in terms of natural frequencies and mode shapes. The approach to account for nonlinear wave theory using the finite element package ABAQUS [14] is to employ equations of state. But rather than computing a detailed solution in the fluid, the tank–liquid system is modeled at the time for which an overall structural response is required. Several aspects of the tank–liquid system require special attention: the liquid inside the tank is modeled with 2D brick elements with displacements as degrees of freedom. To obtain a stable numerical solution, fictitious properties for nearly incompressible and very low viscosity fluid are imposed. The bulk response of the liquid is modeled by a linear equation of state and a Newtonian viscous shear model.

The equations of state in the tank–liquid model provide a hydrodynamic material model that determines the material volumetric strength and the pressure (positive in compression) as a function of the fluid density and the specific energy (internal energy per unit mass). The linear equations of state, known as Mie-Gruniesen equations, use a linear relationship between the shock velocity (U_s) and the particle velocity (U_p), in which

$$P = K\eta, \tag{6}$$

where $\eta = 1 - \rho_o/\rho$, and ρ_o, reference density. This constitutive relation is the same as Eq. (2) in the acoustic medium. The nonlinearity in the model arises from the computation of the volumetric strain, because geometric nonlinearity is introduced in the nonlinear kinematic relations. As the bulk modulus for water is large ($K = 2.07$ GPa), the liquid is almost incompressible. ABAQUS [14] recommends choosing elastic bulk modulus two or three orders of magnitude smaller than the actual value, still holding the near incompressible assumption. A bulk modulus of 2.07 MPa, three orders of magnitude less than the actual bulk modulus of water has been adopted here, as recommended in ABAQUS [14].

Since water is inviscid, the shear viscosity (v) should be small. A viscous shear behavior was adopted, in which the deviatoric stress (S) was described by the Navier–Poisson Law of a Newtonian fluid

$$S = 2ve_p, \tag{7}$$

where e_p is the deviatoric part of the strain rate.

The typical liquid mesh for the nonlinear wave theory model used is presented in Fig. 3, including the boundary conditions along with the interaction between the liquid body and the rigid tank. A total of 560 elements were used to model the liquid and 487 rigid elements for the tank, with a total of 2193 degrees of freedom. The element used to model the liquid body is designated as CPE4R. This is a plane strain element with four nodes, two displacement degrees of freedom per node, bilinear interpolation within the element and reduced integration. The rigid tank shown in Fig. 3 is modeled with element R2D2, which is a 2D linear rigid link for plane elasticity. The interaction between the rigid tank and the solid elements is accounted for by normal contact. The contact between the surfaces uses the master–slave approach, in which the rigid surface is the master and the liquid boundary is the slave. The height of the tank (H) shown in Fig. 3 was sufficiently large for the sloshing wave to form without constraints and to avoid instabilities.

A free surface boundary condition is used, i.e., both normal and shear stresses at the deformed surface are zero, so that the liquid surface can oscillate without restrictions to form sloshing modes. Furthermore, there are no constraints on wave amplitude. This implicitly satisfies Eq. (5) as follows: (a) a body force is initially applied to all 2D elements to represent the self-weight of the liquid; (b) as an initial condition, the hydrostatic vertical and lateral pressures are specified in all 2D elements; (c) at the initial time, the hydrostatic pressures are in equilibrium with the self-weight applied to the 2D elements. As the base excitation is applied in a sloshing frequency, sloshing waves form due to the presence of gravity. The total pressures computed in the analysis are the contact pressures on the rigid wall boundaries, and the sloshing hydrodynamic pressure is obtained by subtracting the hydrostatic pressure from the total pressure.

Since large changes may occur in the domain as the liquid moves, it is necessary to follow the deformation in the system by means of adaptive meshing in ABAQUS [14].

The equation of dynamic equilibrium to solve with the finite element model is described as [15]

$$M^{NM}\ddot{u}^M + I^N - P^N = 0, \tag{8}$$

where $\ddot{u}^M$ is the nodal relative acceleration vector with respect to the base acceleration. M^{NM} is the consistent mass matrix obtained by consistent use of interpolation (diagonal) in explicit formulation, and is given by $M^{NM} = \int_V \rho N^N N^M \,\mathrm{d}V$, where N^N is the vector containing the shape functions of the element; I^N is the internal force vector, computed as the scalar product, $I^N = \int_V (\beta^N : \sigma)\,\mathrm{d}V$, where β^N defines the strain variations of the kinematic variables, σ is the element stress. Finally P^N is the external force vector given by $P^N = \int_S N^M f \,\mathrm{d}s + \int_V N^N F \,\mathrm{d}V$, where f is the applied surface load and F the applied body force.

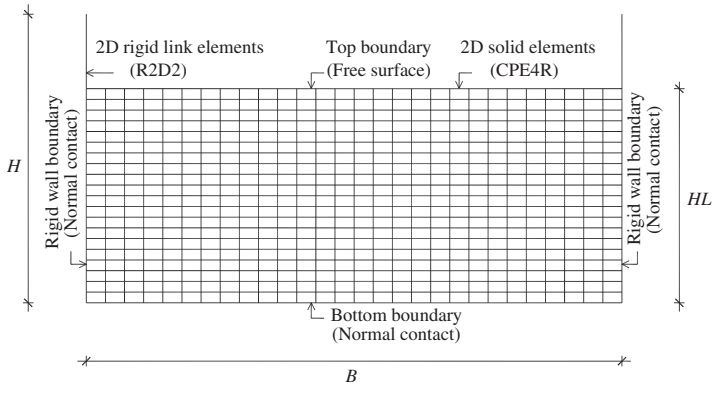

Fig. 3. Typical 2D rectangular model considering nonlinear wave theory.

To obtain the sloshing pressures, a nonlinear harmonic response analysis is carried out, in which the model is subjected to a sinusoidal base excitation ($\ddot{X}_g$), the frequency of the excitation (ω_i) is successively modified using regular intervals, and the surface wave amplitude is recorded. Including the base acceleration in Eq. (8), the dynamic equilibrium equation becomes

$$M^{NM}\ddot{u}^M + I^N = P^N - M^{NM}\ddot{X}_g, \tag{9}$$

where $\ddot{X}_g = \text{HPGA} \sin \omega_i t$, HPGA (horizontal peak ground acceleration) $= 0.01g$, ω_i, input ground motion frequency considered in each analysis.

The volumetric response of the liquid, the low viscous shear stresses, and the contact forces, enter in the calculation of the internal stresses I^N (Eq. (9)). The prescribed hydrostatic pressure and the external body forces are included in the external force vector.

The different harmonic response analyses, performed for the nonlinear wave theory models use the explicit formulation to solve the dynamic equilibrium equations, which is a much faster technique than the standard implicit formulation to solve this kind of problems. This consideration is relevant, since a total of about 40 cases are required to construct a response curve for each model, in order to find the peaks for each of the sloshing modes found. In the explicit formulation, numerical damping is introduced in the solution in the form of bulk viscosity, associated with the volumetric strain. A bulk viscosity pressure (p_{bv1}) is generated to damp the ringing in the highest element frequency, as described in ABAQUS [15]. A linear form of bulk viscosity was used in the tank–liquid model [15]

$$p_{\text{bv1}} = b_1 \rho c_d L_e \dot{\varepsilon}_{\text{vol}}, \tag{10}$$

where b_1 is the damping coefficient; c_d the current dilatational wave speed; and L_e the characteristic length of an element. The bulk viscosity forces are also included in the computation of the internal force (I^N), in Eq. (9). As it turns out from the numerical examples considered in the following section, the natural periods of tanks with a wide range of aspect ratios that were analyzed are not sensitive to variations of wave amplitude within the range of practical relevance. This result justifies the previously stated scope of this paper to analyze the natural frequencies and pressure distributions rather than dealing with the discussion of the wave amplitudes.

3. Natural periods and mode shapes

For each one of the tank–liquid systems listed in Table 1, the first three sloshing natural periods are computed using linear and nonlinear wave theory. The nonlinear effect that the surface wave amplitude has on each of the first three sloshing natural periods is investigated in this section.

3.1. Numerical results for models with linear wave theory

A typical response curve showing the variation of the pressure at the static or original free surface as a function of the excitation period, obtained from the harmonic response analysis in the frequency domain, is presented in Fig. 4, for the tank–liquid system with $H_L/R = 1.65$. The peak in surface pressure, which identifies the first sloshing mode, is much larger than the peaks of the second and third sloshing modes. Since no damping or viscosity is accounted for in the numerical model, the amplitude of all the peaks associated with the natural frequencies should in theory be unbounded; however, due to the discrete nature of the frequencies for which the calculations are carried out, the peaks may turn out of different amplitude depending on the proximity of the discrete frequencies to the natural frequencies of the numerical model. This supports the hypothesis commonly used in the study of sloshing hydrodynamic response that only the first sloshing mode is assumed to predict the sloshing pressures. Therefore, the sloshing pressure contributions of modes higher than the first one can possibly be neglected in the computation of the sloshing pressures or the surface wave amplitude in general cases of broad-band seismic excitations. Similar curves were also constructed for the different tank–liquid systems considered in this study.

The pressure distributions at the liquid surface are shown in Fig. 5. The relation between the surface pressure and the amplitude of the wave formed at the liquid surface was previously stated in Eq. (5).

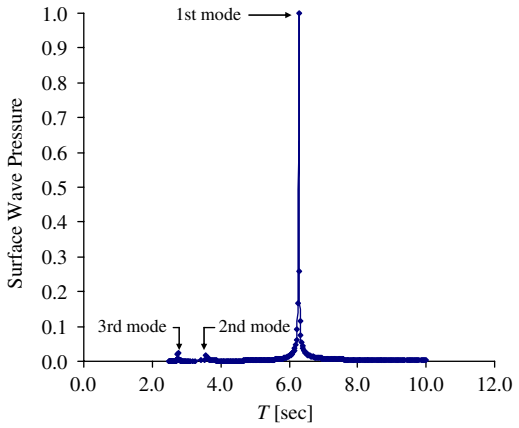

Fig. 4. Modal surface pressure response for the tank–liquid system with $H_L/R = 1.65$; T = natural period.

The natural periods for the first three anti-symmetric sloshing modes, obtained from the peaks of the response curves for the different tank–liquid systems, are presented in Table 2. The peaks of response that represent the natural frequencies were determined by calculating the steady-state response at approximately 0.0004 Hz increments. The first sloshing natural period decreases with the ratio H_L/R, as a natural period of 8.38 s was found for $H_L/R = 0.40$, decreasing to a value of 6.28 s for $H_L/R = 1.65$. In the case of the second and third anti-symmetric modes, similar natural periods were found regardless of the H_L/R ratio. For the second mode, the natural period decreased from 3.70 to 3.57 s, for the models with $H_L/R = 0.40$ and 1.65, respectively. In the case of the third mode, the lowest reduction was obtained, as natural periods of 2.78 and 2.76 s were found.

3.2. Numerical results for models with nonlinear wave theory

The maximum surface wave, as a function of the base acceleration frequency, was obtained for each of the tank–liquid systems considered in the study, for a total time of 40 s, which produces about four cycles of input motion in the first natural period for any of the tank–liquid systems considered. The maximum surface wave response, as a function of the base excitation frequency, is presented in Fig. 6 for the system with $H_L/R = 0.70$. Similar plots of maximum surface wave responses were constructed for the rest of the systems [16]. The maximum surface wave height of the first mode is about five to six times that of the second mode, and about ten times that of the third mode; thus, the sloshing response is dominated by the first sloshing mode. The first three sloshing natural periods for several tank–liquid systems are listed in Table 3. The first period decreases with an increase in H_L/R, but remains constant with H_L/R for the second and third modes.

For the first mode, the time variation of the maximum sloshing wave is shown in Fig. 7 for the system with $H_L/R = 0.70$. The surface wave increases after each cycle, indicating that a resonance period has been found. Fig. 8 shows the shape in the first sloshing mode for the NLWT model with $H_L/R = 0.70$, at two different time steps. The adaptive meshing technique maintains a well-structured mesh as the sloshing surface wave is formed, so that the elements do not have large distortions. Deformed shapes corresponding to the second and third modes for $H_L/R = 0.70$ are presented in Fig. 9, and the amplitudes are much smaller than in the first sloshing mode.

A summary of the natural periods for the first three sloshing modes with linear and nonlinear wave theory, previously presented in Tables 2 and 3, is shown in Fig. 10. Similar natural periods were obtained with linear and nonlinear wave theory for the first three modes with differences less than 2%, 3.5%, and 4.8% for the first, second, and third sloshing modes of the rectangular models. Therefore, one may conclude that nonlinearity does not have significant effects on the natural periods.

To further investigate the effect of the surface wave amplitude on the first sloshing natural period, the tank–liquid systems were analyzed for a total time of 100 s, which produced about 11 cycles of input motion. For the models with $H_L/R = 0.40$, 0.56, 0.87 and 1.10, the first sloshing natural period was measured for each

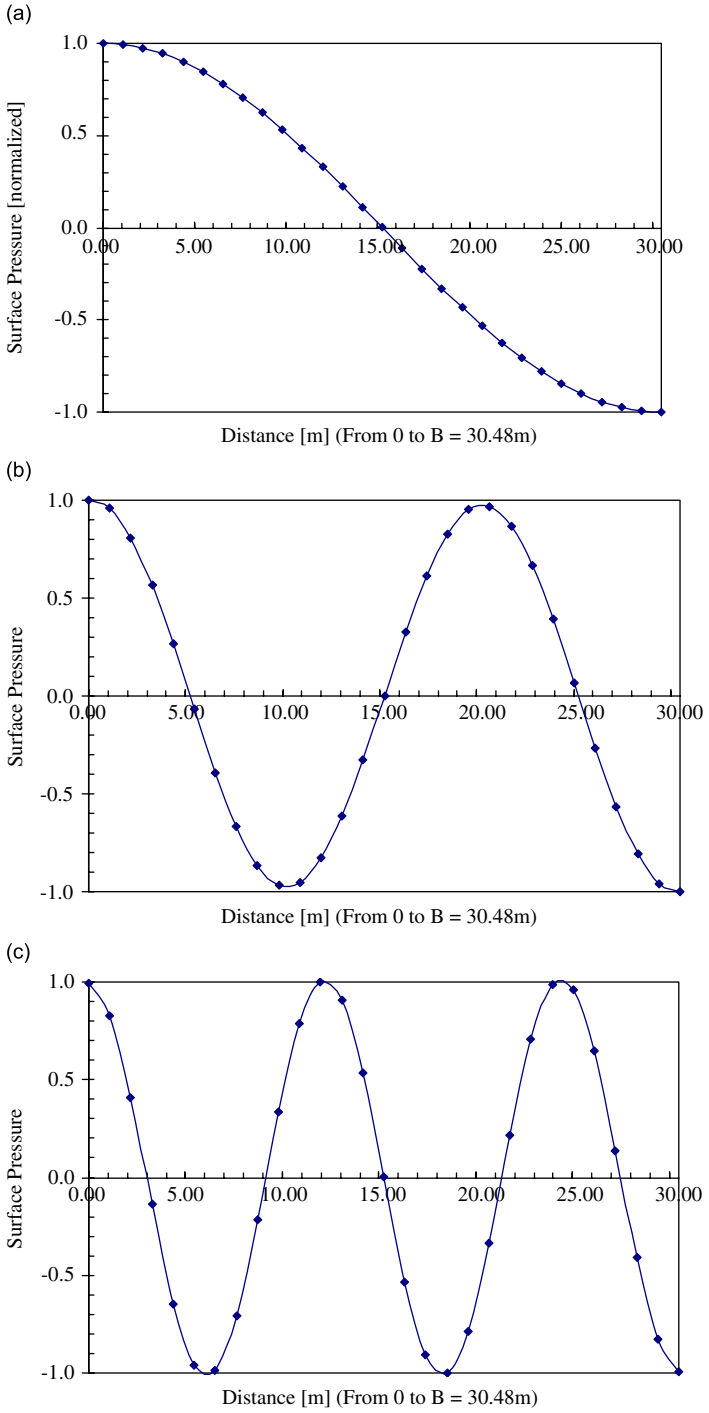

Fig. 5. First three sloshing modes for the 2D linear wave theory model with $H_L/R = 1.65$: (a) first sloshing mode, (b) second sloshing mode, and (c) third sloshing mode. Surface pressures are normalized with respect to the maximum amplitude of each mode.

cycle and plotted in Fig. 11. In Fig. 11 there are only small little variations of the first sloshing natural period with the sloshing wave amplitude. Notice that for all the cases shown in this figure, the maximum surface wave amplitude at the last cycle is larger than 4.5 m for all cases and reaches amplitudes of about 6.5 m in some

Table 2
Sloshing natural periods in seconds for the model with LWT, obtained from the steady state harmonic analyses

Model	H_L/R	Sloshing modes		
		First	Second	Third
1	0.40	8.38	3.70	2.78
2	0.56	7.45	3.62	2.78
3	0.63	7.19	3.62	2.78
4	0.70	6.99	3.62	2.78
5	0.87	6.67	3.62	2.77
6	0.95	6.58	3.62	2.77
7	1.10	6.46	3.57	2.77
8	1.27	6.37	3.57	2.76
9	1.65	6.28	3.57	2.76

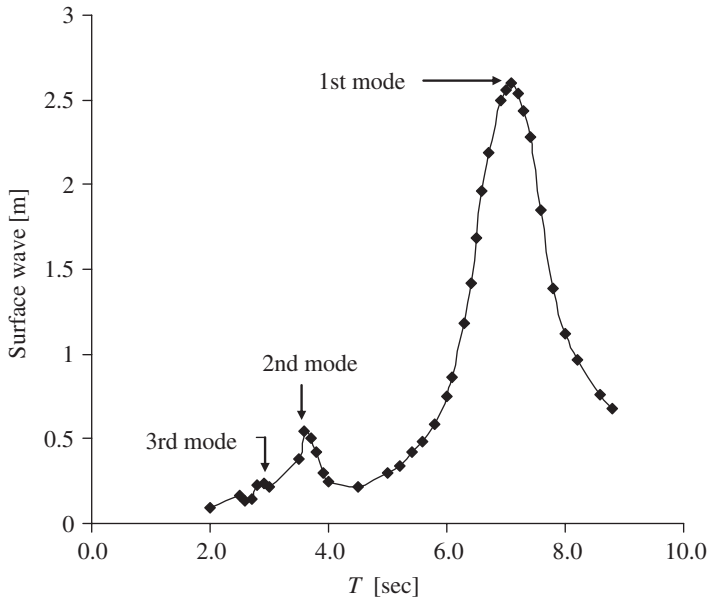

Fig. 6. Maximum surface wave displacement for the tank–liquid system with $H_L/R = 0.70$.

Table 3
Natural periods in seconds for the first three sloshing modes, computed with NLWT

Model	H_L/R	Sloshing modes		
		First	Second	Third
1	0.40	8.50	3.70	2.90
2	0.56	7.60	3.70	2.90
3	0.63	7.30	3.70	2.90
4	0.70	7.10	3.60	2.90
5	0.87	6.70	3.70	2.90
6	0.95	6.50	3.60	2.90
7	1.10	6.50	3.70	2.90
8	1.27	6.40	3.60	2.90
9	1.65	6.40	3.70	2.80

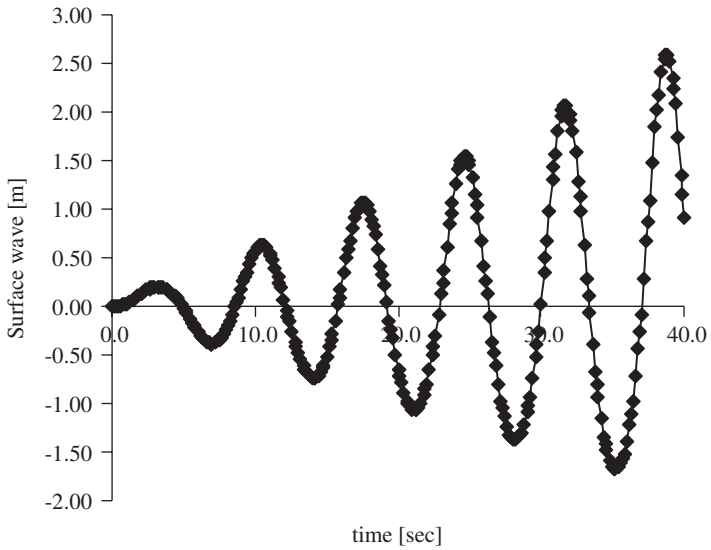

Fig. 7. Variation in time of the surface wave in the first sloshing mode for the model with $H_L/R = 0.70$.

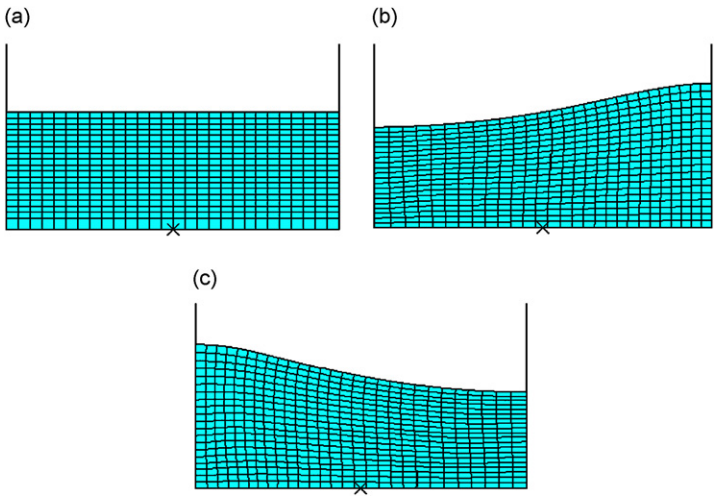

Fig. 8. Liquid shapes corresponding to the first sloshing mode for the tank–liquid system with $H_L/R = 0.70$: (a) $t = 0$, (b) $t = 35.2$ s ($d_{\min} = -1.67$ m), and (c) $t = 38.8$ s ($d_{\max} = 2.59$ m).

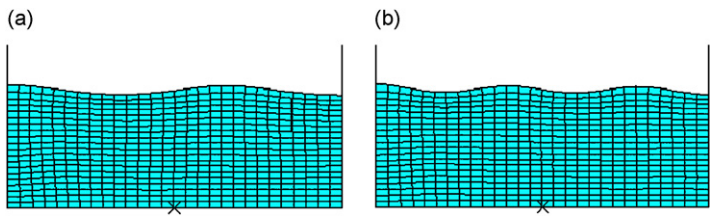

Fig. 9. Liquid shapes corresponding to the second and third sloshing modes for the tank–liquid system with $H_L/R = 0.70$: (a) second mode, $d_{\max} = 0.472$ m, $t = 38$ s, and (b) third mode, $d_{\max} = 0.239$ m, $t = 30.4$ s.

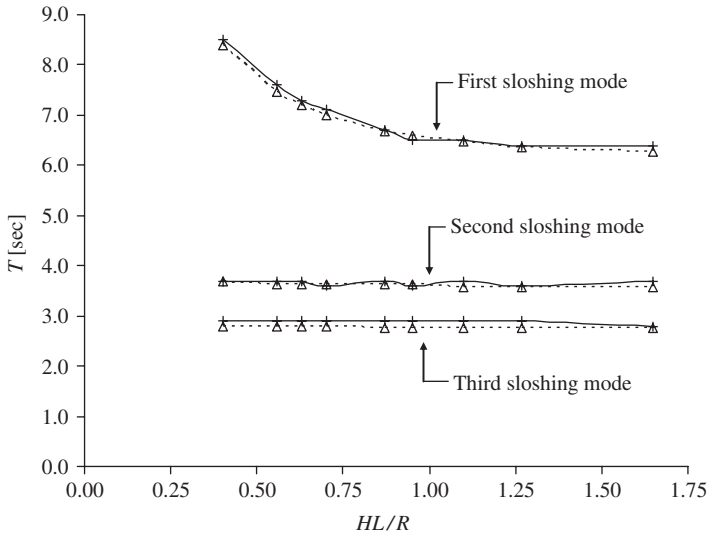

Fig. 10. Comparison of the first three sloshing natural periods for the tank–liquid systems considering linear and nonlinear wave theory. ——+——, Nonlinear; - - -△- - - linear.

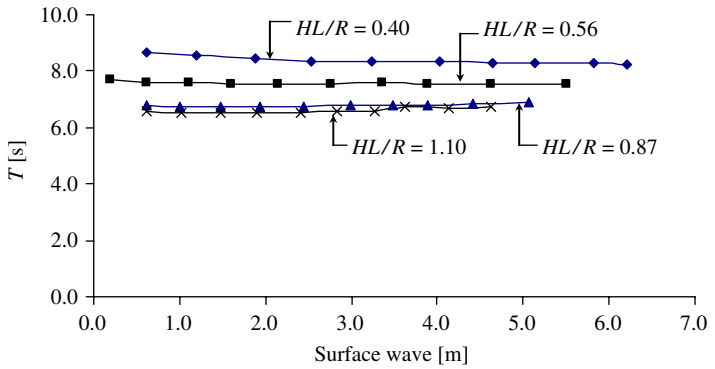

Fig. 11. Variation of the first sloshing natural period with the surface wave amplitude for models with different H_L/R ratios.

cases. Therefore, up to the surface wave amplitudes computed, the first sloshing natural period was practically independent from the surface wave amplitude.

3.3. Simplified expressions for sloshing natural periods of rectangular tanks

The sloshing natural periods and modes obtained with both LWT and NLWT in the preceding section can also be approximated for various height/width ratios by means of a physical analogy between the sloshing modes and the natural periods of the fluid undergoing rigid motions in the case of a tank with a half circular cross section.

The fundamental mode of vibration of the half circular cylindrical tank coincides exactly with the rigid body rotational oscillation of the fluid around the axis of the cylinder acting as a pendulum. The natural period of small amplitude rigid body oscillation in the gravity field is given by the expression

$$T_1 = 2\pi\sqrt{\frac{r}{g}}, \tag{11}$$

where r is the radius of inertia of the fluid mass about the center of the circular cross section of radius R, given by $r = 3/16\pi R$, and Eq. (11) can be rewritten as

$$T_1 = 2\pi\sqrt{0.589\frac{R}{g}}. \tag{12}$$

Since this mode corresponds to a rigid body motion, the free fluid surface remains a straight line during the oscillations. At this point it is of interest to compare the fundamental period of the tank with a rectangular cross section analyzed in Tables 2 and 3 for the aspect ratio $\beta = H_L/R = 1$ (by linear interpolation between $\beta = 0.95$ and $= 1.10$) with that given by Eq. (12):

- T_1 of half cylinder: 6.01 s.
- T_1 of rectangular tank: 6.54 s from Table 2, or 6.50 s from Table 3.

Similarly, for $\beta = 1.65$ the values of T_1 for the rectangular tanks from Tables 2 and 3 are 6.28 and 6.4 s, respectively. These numerical results exhibit a tendency to an asymptotic value of about 6.20 s for very deep rectangular tanks, which is only about 3% away from that of the half cylindrical tank.

In view of this correspondence between the rectangular and half cylindrical cross section cases, one should expect that the higher anti-symmetric sloshing modes for the rectangular tank will have natural frequencies close to the asymptotic value for deep rectangular tanks multiplied by $\sqrt{1/3}$ (second mode), $\sqrt{1/5}$ (third mode), etc., i.e., 3.6, 2.8 s, and so on. These values are in close agreement with those given in Tables 2 and 3 for the higher asymmetric modes. This correspondence holds even for tanks of smaller depth/width ratios ($\beta < 1$), since for higher modes the asymptotic condition of deep tanks applies for a wider range of β than for the fundamental mode.

For relatively shallow rectangular tanks, it is possible to extend the rigid body pendulum oscillation associated with the fundamental sloshing mode by considering a rigid body cross section in the form of half an ellipse, or a slender rectangular strip. Such approximations may be found useful for preliminary calculations of the sloshing fundamental period for tanks with $\beta < 1$ as a complement to the previously discussed Analogy of the half cylinder for deep rectangular tanks ($\beta \geqslant 1$). The aforementioned approximation of the fundamental period for shallow rectangular tanks leads to the following expressions:

$$T_1 = 2\pi\sqrt{c\frac{R}{g}}, \tag{13}$$

where the value of c is given by $c = \beta(0.589) + 3/4\pi((1-\beta)(1+\beta)^2)/4\beta$ considering the assumption of a half-ellipse rigid cross section, and $c = \beta(0.589) + 2(1-\beta)/3\beta$ considering the assumption of a rectangular strip rigid cross section. The fundamental sloshing period obtained with the proposed approximations for shallow tanks is given in Table 4 together with the results with finite elements analysis using linear and nonlinear wave theory.

Table 4
Fundamental sloshing period (T_1) in seconds for shallow rectangular tanks

β	FE LWT	FE NLWT	Approximation of fluid as rigid half ellipse	Approximation of fluid as rigid rectangular strip
0.4	8.38	8.50	8.79	8.71
0.56	7.45	7.60	7.58	7.24
0.7	6.99	7.10	6.95	6.54
0.87	6.67	6.70	6.40	6.13
0.95	6.58	6.50	6.16	6.04

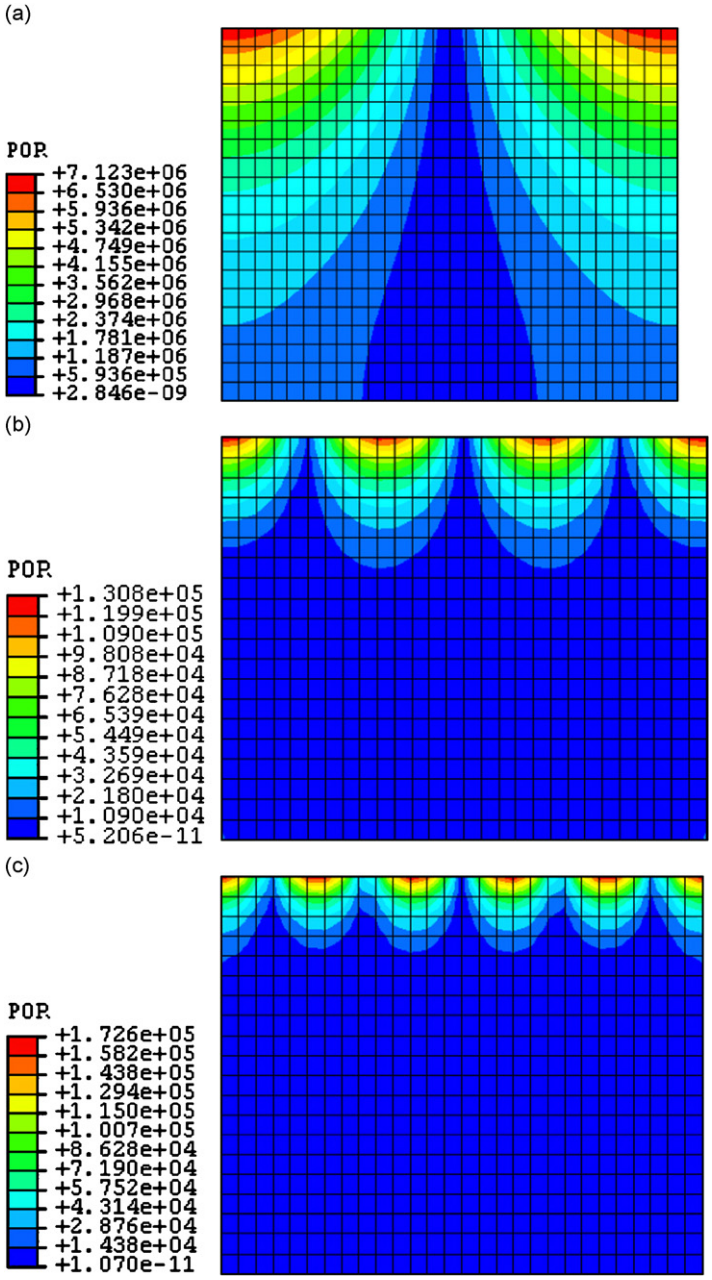

Fig. 12. Pressure contours for the first three modes obtained with LWT for $H_L/R = 1.65$: (a) first mode, (b) second mode, and (c) third mode.

4. Sloshing pressure distribution

The sloshing pressure distributions obtained with linear and nonlinear wave theory were normalized with respect to the maximum amplitude, so that they could be compared to each other.

4.1. Hydrodynamic pressure distribution considering linear wave theory

Pressure contours were plotted for the harmonic response analysis of the rectangular model (similar to that shown in Fig. 12), and pressure distributions on the rigid wall were obtained from them. Fig. 13 presents the

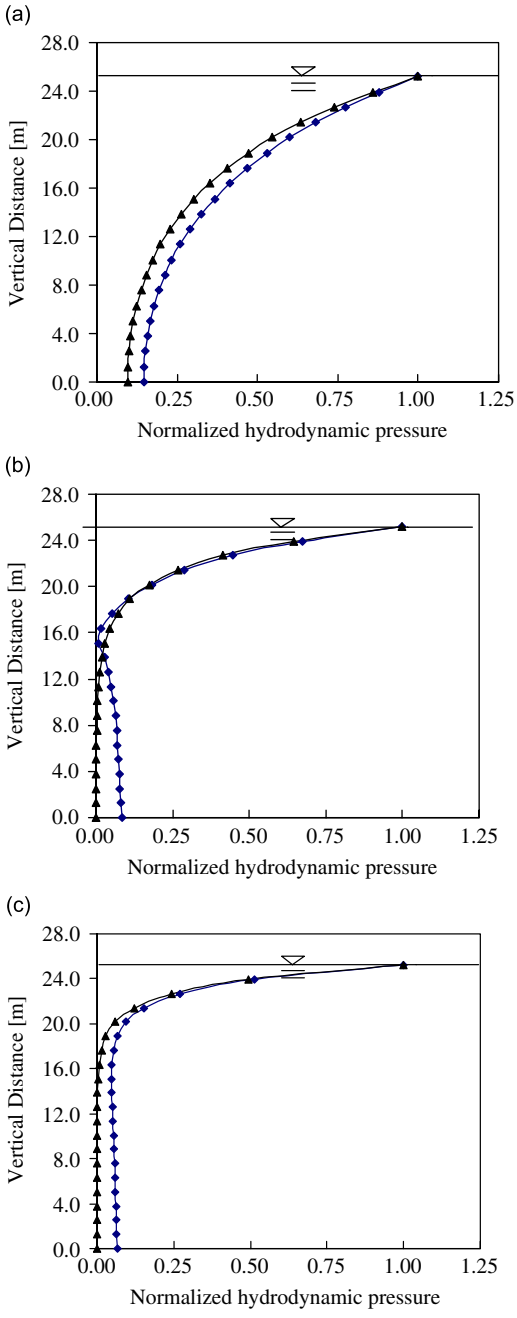

Fig. 13. Comparison of sloshing pressures at the tank wall for the tank–liquid system with $H_L/R = 1.65$: (a) first sloshing mode, (b) second sloshing mode, and (c) third sloshing mode. —●—, LWT model; —▲—, Veletsos and Shivakumar [10].

normalized pressure distributions on the rigid wall for $H_L/R = 1.65$. The pressure resultant is largest for the first mode, and decreases for higher modes. This observation agrees with the peak responses for the different sloshing modes previously presented in Fig. 4, from which a much larger surface pressure is observed for the first sloshing mode in comparison with the second and third sloshing modes. This is the main reason for which the sloshing response is mostly dominated by the first mode.

The pressure distribution on the tank rigid wall was compared with that proposed by Veletsos and Shivakumar [10] for a cylindrical tank. An equation for the convective hydrodynamic pressure distribution for

rigid cylindrical tanks is derived in Ref. [10] under the following assumptions: (a) the liquid is homogeneous, inviscid and incompressible; and (b) the upper liquid surface is free, with a linear relation between the pressure and the sloshing wave height. The tank is anchored to the foundation at its base, resting on rigid soil. The pressure distribution on the tank wall for the case of the rectangular model ($H_L/R = 1.65$) is shown in Fig. 13 with the distribution given by Ref. [10] for the direction of the excitation. Clearly, the pressure distributions shown in Fig. 13 apply to different geometries (rectangular and cylindrical tanks), but the pressure patterns for the first three sloshing modes are similar. This similarity is also present for other H_L/R ratios [16].

4.2. Hydrodynamic pressure distribution considering nonlinear wave theory

As stated in the previous section, in most cases the sloshing response is dominated by the contribution of the first mode. Therefore, the effects of nonlinearity on the pressure distributions are only considered in this section for the pressures due to the first sloshing mode.

The sloshing pressure distribution on the wall, obtained for the first sloshing mode for $H_L/R = 0.40$ and 0.70, are presented in Figs. 14 and 15 for two different sloshing wave heights. These pressure distributions correspond to the case in which a maximum sloshing wave height is obtained at the left rigid wall, thus having a deformed shape similar to that in Fig. 8(c). For $H_L/R = 0.40$ (Fig. 14), the difference between the pressure distributions using linear and nonlinear wave theory decreased for a larger surface wave amplitude. For the remaining tank–liquid systems ($H_L/R = 0.56$–1.65), as the sloshing wave height increases, the difference between the pressure distribution obtained for the LWT and NLWT also increases, as is shown in Fig. 15 for $H_L/R = 0.70$.

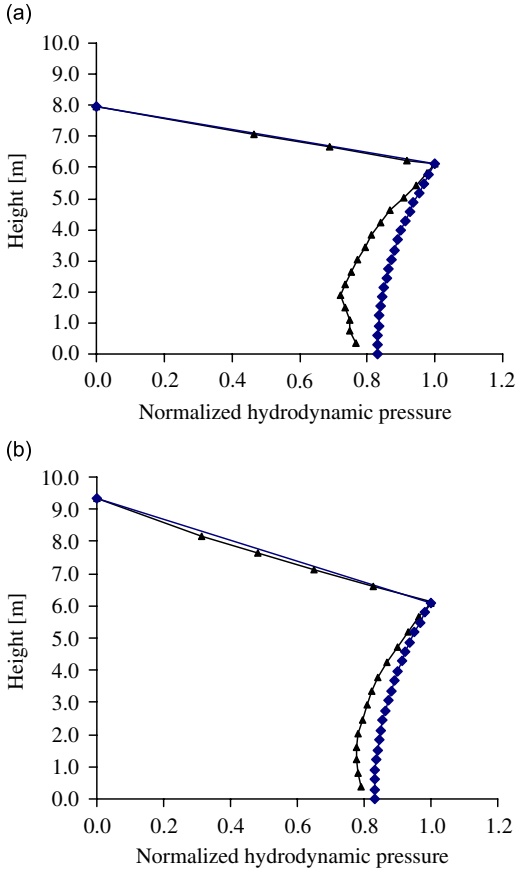

Fig. 14. Pressure distribution for the first sloshing mode of a tank–liquid system with $H_L/R = 0.40$: (a) surface wave = 1.87 m, and (b) surface wave = 3.24 m. —▲—, Nonlinear model; —●—, linear model.

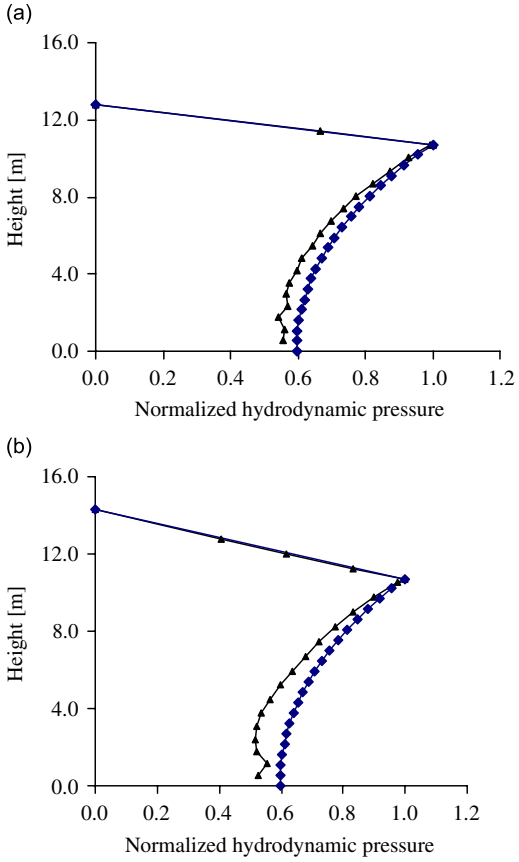

Fig. 15. Pressure distribution for the first sloshing mode of a tank–liquid system with $H_L/R = 0.70$: (a) surface wave = 2.06 m, and (b) surface wave = 3.55 m. ——, Nonlinear model; ——, linear model.

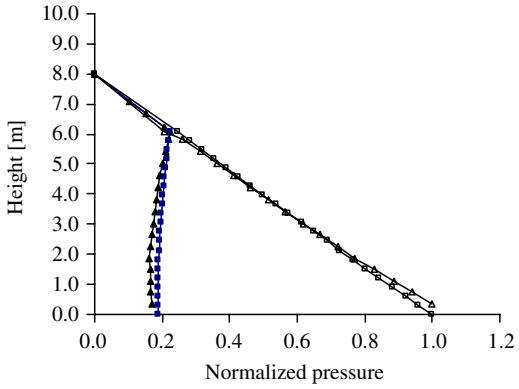

Fig. 16. Total pressure and hydrodynamic pressure distribution for the first sloshing mode of the tank–liquid system with $H_L/R = 0.40$, and a surface wave = 1.87 m. ——, Sloshing hydrodynamic pressure nonlinear wave theory; —— sloshing hydrodynamic pressure linear wave theory; ——, total pressure nonlinear wave theory; ——, total pressure linear wave theory.

The total pressures (hydrodynamic plus hydrostatic) were plotted together with the sloshing pressures in Figs. 16 and 17, for the tank–liquid systems of Figs. 14(a) and 15(a). Here the sloshing pressures from nonlinear and linear wave theory are shown in the scale of the total pressure, and only small differences are observed between the nonlinear and linear models. The total pressures for the linear and nonlinear wave theory models, presented in Figs. 16 and 17, show similar pressure distributions.

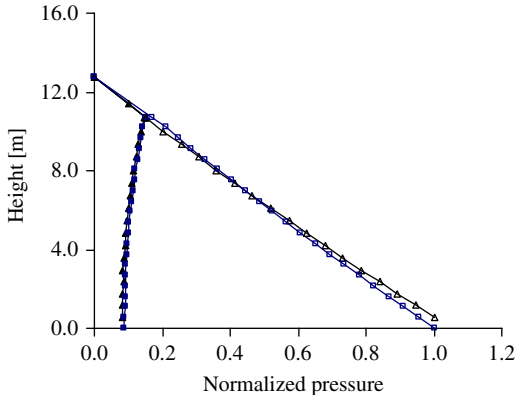

Fig. 17. Total pressure and hydrodynamic pressure distribution for the first sloshing mode of the tank–liquid system with $H_L/R = 0.70$, and a surface wave = 2.06 m. ——△——, Sloshing hydrodynamic pressure nonlinear wave theory; ——■——, sloshing hydrodynamic pressure linear wave theory; ——△——, total pressure nonlinear wave theory; ——□——, total pressure linear wave theory.

In all cases considered in this research, slightly larger values of pressure resultants and lower pressure resultant heights were obtained for the models with LWT. From Figs. 14–17, one can conclude that the nonlinearity due to the large surface wave amplitude does not have major effects in the pressure distributions for the tank walls of rectangular tanks.

4.3. Approximate expressions for total pressures

As shown in Figs. 16 and 17, the total pressure on the tank walls may closely be approximated by means of a linear variation between the point of maximum wave height and that at the bottom approximated by assuming that the effect of the lateral motion is equivalent to statically tilting the tank to make coincide the free surface of the tank with the point of maximum wave elevation at the wall. Other force resultants, such as total base shear or overturning moments on the tank foundations, can also be approximated by those corresponding to the equivalent static tilt that produces the same displacement of the free surface of the liquid on the tank walls. The degree of equivalent tilting is directly defined by the dynamically computed maximum wave height, which in turn is a direct consequence of the ratio of the forcing frequency to the fundamental sloshing mode frequency, and of the number of cycles of excitation, particularly in the case of resonance or near resonance.

5. Conclusions

The first sloshing natural period for rectangular tanks considering linear wave theory decreases with H_L/R up to $H_L/R = 0.80$, and then remains almost constant for larger ratios of H_L/R. The second and third anti-symmetric sloshing natural periods remain almost constant regardless of H_L/R. These results are discussed in conjunction with the analogy between the sloshing motions and a physical pendulum, and simplified expressions to estimate the fundamental and higher anti-symmetric frequencies for both deep and shallow rectangular tanks were also presented.

The amplitude of the first sloshing mode for a resonant frequency is much higher than for the other modes, and this conclusion applies to both linear and nonlinear wave theory. The same variation with H_L/R was observed for the first three sloshing modes, as linear and nonlinear wave theory were considered for the rectangular model. The nonlinearity in the rectangular tank did not have significant effects on the sloshing natural period, with differences smaller than 5% for all the tank–liquid systems considered. This conclusion states for maximum surface wave amplitudes in the order of 4.50–7.0 m, and the range of H_L/R ratios used in this study.

Similar sloshing pressure distributions for the first three sloshing modes were obtained for the linear wave theory rectangular models and those proposed in Veletsos and Shivakumar [10] for cylindrical tanks.

The pressure resultants in both cases were much larger for the first sloshing mode, and decreased for higher sloshing modes.

For the first sloshing mode, slightly larger values of pressure resultants and lower pressure resultant heights were obtained for the models with linear wave theory in comparison with that predicted using nonlinear wave theory. It is concluded that the nonlinearity of the surface wave amplitude does not have major effects on the pressure distribution on the walls of rectangular tanks.

Acknowledgments

Virella was supported by a PR-EPSCOR post-doctoral fellowship Grant EPS-0223152 for this research. Godoy was a member of the research staff of CONICET during this research.

References

[1] H.M. Koh, J.K. Kim, J.H. Park, Fluid-structure interaction analysis of 3-D rectangular tanks by a variationally coupled BEM-FEM and comparison with test results, *Earthquake Engineering and Structural Dynamics* 27 (1998) 109–124.
[2] G.W. Housner, The dynamic behavior of water tanks, *Bulletin of Seismological Society of America* 53 (2) (1963) 381–389.
[3] M.A. Haroun, Stress analysis of rectangular walls under seismically induced hydrodynamic loads, *Bulletin of Seismological Society of America* 74 (3) (1984) 1031–1041.
[4] A.S. Veletsos, Seismic effects in flexible liquid-storage tanks, *Proceedings of the Fifth World Conference on Earthquake Engineering*, Rome, Italy, 1973, pp. 630–639.
[5] A.S. Veletsos, Seismic response and design of liquid storage tanks: Guidelines for the seismic design of oil and gas pipeline systems, *ASCE Technical Council on Lifeline Earthquake Engineering*, New York, 1984, pp. 443–461.
[6] A.S. Veletsos, J.Y. Yang, Earthquake response of liquid storage tanks—advances in civil engineering through mechanics, *ASCE Proceedings of the Second Engineering Mechanics Specialty Conference*, Raleigh, NC, 1977, pp. 1–24.
[7] M.A. Haroun, G.W. Housner, Seismic design of liquid storage tanks, *Journal of Technical Councils* 107 (1) (1981) 191–207.
[8] J.K. Kim, H.M. Koh, I.J. Kwahk, Dynamic response of rectangular flexible fluid containers, *Journal of Engineering Mechanics* 122 (1996) 807–817.
[9] Y.S. Choun, C.B. Yun, Sloshing Analysis of rectangular tanks with a submerged structure by using small-amplitude water wave theory, *Earthquake Engineering and Structural Dynamics* 28 (1999) 763–783.
[10] A.S. Veletsos, P. Shivakumar, Tanks containing liquids or solids, in: D.E. Beskos, S.A. Anagnostopoulos (Eds.), *Computer Analysis and Design of Earthquake Resistant Structures: a Handbook*, vol. 3, Computational Mechanics Publications, Southampton, UK, 1997, pp. 725–773.
[11] N.M. Newmark, E. Rosenblueth, *Fundamentals of Earthquake Engineering*, Prentice-Hall, Englewood Cliffs, NJ, 1971.
[12] H.D. Hibbit, B.I. Karlsson, P. Sorensen, *Structural-Acoustics Analysis using ABAQUS*, Hibbit, Karlsson and Sorensen Inc., Rhode Island, 2002.
[13] ABAQUS/Standard version 6.4 User's Manual, Hibbit, Karlsson and Sorensen Inc., Rhode Island, 2002.
[14] ABAQUS/Explicit version 6.4 User's Manual, Hibbit, Karlsson and Sorensen Inc., Rhode Island, 2002.
[15] ABAQUS/Theory version 6.4 User's Manual, Hibbit, Karlsson and Sorensen Inc., Rhode Island, 2002.
[16] J.C. Virella, Buckling of Steel Tanks Subject to Earthquake Loadings, Ph.D. Thesis, University of Puerto Rico at Mayagüez, 2004.